Clinical application of 3D virtual and printed models for cerebrovascular diseases

Jin Woo Bae
Seoul National University Hospital
Da Yeong Lee
MEDICALIP Co. Ltd
Chang Hwan Pang
Seoul National University Hospital
Jeong Eun Kim
Seoul National University Hospital
Chul-Kee Park
Seoul National University Hospital
Doohee Lee
MEDICALIP Co. Ltd
Sang Joon Park
Seoul National University Hospital
Won-Sang Cho (nsdrcho@gmail.com)
Seoul National University Hospital

Research Article

Keywords: intracranial aneurysms, 3D, cerebrovascular diseases, consisting of 9 intracranial aneurysms, 2 cavernous malformations

Posted Date: January 8th, 2021

DOI: https://doi.org/10.21203/rs.3.rs-140296/v1

Clinical application of 3D virtual and printed models for cerebrovascular diseases

Jin Woo Bae, MD,[1] Da Yeong Lee, MS,[3] Chang Hwan Pang, MD,[1] Jeong Eun Kim, MD, PhD,[1] Chul-Kee Park, MD, PhD,[1] Doohee Lee, MS,[3] Sang Joon Park, PhD,[2,3*] Won-Sang Cho, MD, PhD[1*]

Departments of Neurosurgery[1] and Radiology[2], Seoul National University Hospital, Seoul, Korea

[3]MEDICALIP Co. Ltd., Seoul, Republic of Korea

Correspondence:

Won-Sang Cho, MD, PhD

Associate Professor

Department of Neurosurgery, Seoul National University Hospital

Daehak-ro 101, Jongno-gu, Seoul 03080, Republic of Korea

Tel: +82-2-2072-2824, Fax: +82-2-744-8459

E-mail: nsdrcho@gmail.com

Sang Joon Park, PhD

Research Associate Professor

Department of Radiology, Seoul National University Hospital

Daehak-ro 101, Jongno-gu, Seoul 03080, Republic of Korea

Tel: +82-2-3668-7952, Fax: +82-2-743-6385

E-mail: lunao78@snu.ac.kr

Clinical application of 3D virtual and printed models for cerebrovascular diseases

Abstract

Three-dimensional (3D) printing techniques are rapidly advancing in the medical industry and in clinical practice. We aimed to evaluate the usefulness of 3D virtual and printed models of 12 representative cerebrovascular diseases, consisting of 9 intracranial aneurysms, 2 cavernous malformations and 1 arteriovenous malformation. Using the software we developed, segmentation of raw data and rendering and modification for 3D virtual models were processed mostly automatically. Among the 12 virtual models, 9 (excluding 3 intracranial aneurysms) were printed with a commercial 3D printing system and materials. Most intracranial structures were satisfactorily made, including the skull, brain, vessels, thrombus, tentorium and major cranial nerves. The 3D models were thought to be very helpful in experiencing the operative views from various directions in advance and in selecting an appropriate surgical approach. However, it was still difficult to discriminate small vessels and cranial nerves, to feel a realistic tactile sense and to directly perform presurgical simulations, such as dissection, removal, clipping and microanastomosis. With advancements in radiological resolution, processing techniques and material properties, 3D modeling is expected to simulate real brain tissues more closely.

Introduction

Since Charles Hull filed US patents for the world's first 3-dimensional (3D) printer in 1984,[1] 3D printing techniques have rapidly expanded throughout different industries. 3D printing was first applied for dental implants in the 1990s, and thereafter it has been innovatively adopted in a few medical fields, such as anatomical models for surgery and education, devices and instruments for drug delivery and surgery, implants and prostheses, and bioprinting.[2] Despite the advancement of neuroimaging, it is still not easy to recognize the intracranial structures and their 3D relationships because they are minute and complex and are found within a narrow space. Therefore, in the field of neurosurgery, the cultivation of mental processing ability through repetitive experience and learning has been very important in understanding 3D neuroanatomy and in achieving satisfactory surgical outcomes. In that sense, 3D printing is expected to become a practical solution to shorten the learning curve and improve surgical results.

There have been many attempts to apply 3D printing techniques to presurgical planning, education, and the development of devices and implants in a few neurosurgical fields, such as cerebrovascular diseases, brain tumors, spinal diseases, functional disorders, congenital anomalies and neurotrauma.[2,3] In the area of cerebrovascular diseases, studies have continued since the first report by D'Urso et al. in 1999[4] that mainly dealt with intracranial aneurysms (IAs) and arteriovenous malformations (AVMs).[3-15] We evaluated the usefulness and limitations of 3D printing techniques by making 3D virtual and printed models of representative cerebrovascular diseases such as IA, AVM and cavernous malformations (CM) using our brand-new software for segmentation and rendering.

Patients and Methods

Patients

The baseline characteristics of 9 intracranial aneurysms (IAs), 2 cavernous malformations (CMs) and 1 arteriovenous malformation (AVM) are summarized in **Table**. They were selected in terms of how delicate and realistic the 3D models of these cerebrovascular diseases and intracranial structures would be and how helpful they would be in selecting an appropriate surgical approach. Except for Case 9, in which 3D virtual and printed models were created preoperatively, the 3D models in the other 11 patients were made retrospectively. This study included adult patients who had undergone cerebrovascular surgery at Seoul National University Hospital (Seoul, Korea). The study protocol was approved by the Institutional Review Board of Seoul National University Hospital (IRB number: 2007-090-1141). This study was also conducted in accordance with the principles of the Declaration of Helsinki. Because this present study only used the routinely acquired patient data and had no risks to enrolled patients, the requirement for individual informed consent was waived by our Institutional Review Board.

Among the 9 patients with IAs, 7 patients with unruptured aneurysms were treated via various kinds of keyhole approaches, such as supraorbital approaches (frontolateral supraorbital craniotomy [FL] and lateral supraorbital craniotomy [LSO]), minipterional (MP) and mini-interhemispheric (MI) approaches.[16] The other 2 IA patients presented with subarachnoid hemorrhage and mass effect, respectively, which were treated with conventional craniotomy and aneurysmectomy/aneurysmorrhaphy or bypass/distal trapping. Two CMs were completely removed via conventional approaches because they presented with repeated bleeding and subsequent neurological decline. One patient with an AVM presented with intracerebral and intraventricular hemorrhage, and it was completely removed via a large craniotomy.

Segmentation for 3D Virtual Modeling

The first step was to create software that could accurately segment the anatomical structures of the skull, brain and vessels. The manual drawing method using threshold

differences was unavoidable in some parts of the segmentation process due to the complexity of intracranial structures. However, most of the segmentation process was automated using a program that performs segmentation, reconstruction and rendering based on machine learning-based threshold, region growing and graph-cut algorithms (MEDIP®, http://medicalip.com/shop/medip.php, MEDICALIP, Seoul, Republic of Korea). When axial source DICOM images of computed tomographic angiography (CTA), magnetic resonance (MR) and 3D rotational angiography (3DRA) data from digital subtraction angiography (DSA) were registered in MEDIP®, preprocessing to remove noise generated in the medical images was performed. Subsequently, the specified region of interest was replaced with seed information when the user designated the region of interest, and segmentation was performed for the area with the same seed information using a graph-cut algorithm, which is the core algorithm of MEDIP® software. Then, optimization was carried out, considering that 3D medical images should be segmented within the actual distance (spacing) between each pixel and given the limited number of pixels and thus limited resolution. Fully and semiautomated segmentations were performed by the function named draw cut in MEDIP®. Using the multiplanar reconstruction function of MEDIP®, the 3D virtual models of the cerebrovascular diseases and the radiological images could overlap at the desired reference point so that segmentation could proceed while confirming that the process has been performed correctly. As the source images for segmentation, we used a combination of CTA; 3-tesla MR images with T1- and T2-weighted, T2 fluid-attenuated inversion-recovery and time-of-flight MR sequences; and 3DRA. All the source images were taken with various-thickness slabs and spaces (MR, 0.5 – 1 mm; CTA, 1 mm; 3DRA, 0.12 mm)

Primary Rendering and Modification of 3D Virtual Models

The 3D virtual models that are primarily rendered after segmentation can be shared with physicians and manufacturers in an interactive way on the website by the mobile MEDIP app (MODIP®, MEDICALIP, Seoul, Republic of Korea). MODIP® is a tool for real-

time communication using a smartphone or computer, through which the prototypes of 3D virtual models can be shared and modified (**Table**). It has some useful functions: 1) rotating and resizing the 3D models to check their accuracy; 2) entering text labels or drawing some pictures as needed for model modification; 3) changing the colors and transparency of the structures for clear identification; and 4) cropping an ROI in order to print only the desired range. After this interactive process, 3D virtual models for printing finally proceed to the 3D printing step.

Implementation of 3D Printed Models

The production of the patient-specific 3D-printed models consists of 3 stages: 1) creating a stereolithography file for 3D printing; 2) printing a primary model using a 3D printer; and 3) a postprocessing step, including manual editing. Authentic realization of the gyrus and sulcus using transparent silicon materials of a texture similar to that of the brain to see through the intra-axial structures is the key component of our model. However, the diffuse reflection caused by the gyrus and sulcus sometimes disturbs the observation of the internal structures. Therefore, sometimes the surface of printed brain models is deliberately smoothed. After performing the subtraction process using the slicing program to guarantee no overlap among the brain parenchyma, vascular lesions and other structures, they were extracted into separate stereolithography files and printed out independently with the desired materials and colors. The slicing of the brain parenchyma was performed using the Flash Print program (FlashForge; No. 518 XianYuan Road, Jinhua City, ZheJiang Province, China), and gyrus and sulcus-shaped moldings were printed out using acrylonitrile butadiene styrene copolymers by the fused deposition modeling method (Guider 2, [FlashForge; No. 518 XianYuan Road, Jinhua City, ZheJiang Province, China]). The vascular lesions and other structures were sliced using the Grab CAD program (Stratasys; 7665 Commerce Way Eden Prairie, MN 55344, USA) and were printed with photovoltaic resin as the material by the Polyjet method (J750 [Stratasys; 7665 Commerce Way Eden Prairie, MN 55344, USA]). The supporters attached to the outputs were removed after printing, and the brain

parenchyma was fumigated to smoothen the surface. After assembling the gyrus and sulcus-shaped moldings, the outputs of cerebrovascular lesion data and the internal brain structures, the transparent silicone material with brain-mimicking texture was injected into the molding and then dried. After the silicone material had completely dried, the mold was removed, and the 3D-printed model was finished by homogenizing the surface. All the printed models were made at a scale of 1:1.

Results

Aneurysms

Single IAs

***Cases 1 and 2*:** The 3D virtual models of 2 cases were retrospectively made only using CTA, with no 3D-printed modeling. In Case 1, an aneurysm arising from the anterior communicating artery (ACoA) was clipped via the right FL approach. It is standard to approach a target via the side of the dominant A1 for proximal control; however, the nondominant side was more advantageous to clip this case, which was easily imaged on the 3D virtual model (**Figure 1a and b**). In Case 2, a 17.2 mm aneurysm at the right middle cerebral artery (MCA) bifurcation was clipped via the right MP approach. The perisylvian approach was more advantageous than any supraorbital approaches because the aneurysm was large and was located mainly below the sphenoid ridge (**Figure 1c-f**). 3D virtual models seemed likely to help make these judgments intuitive.

Case 3: An aneurysm at the distal anterior cerebral artery (ACA) was clipped via the right MI approach. There are many points to consider when performing the MI approach for distal ACA aneurysms, including the proper head position and location of the craniotomy for approaching the aneurysm and avoiding bridging veins. The 3D virtual and printed models were implemented only from CTA, and they seemed good enough to make decisions on such matters (**Figure 1g-i**).

Multiple IAs

Case 4: Two aneurysms at the right MCA and superior cerebellar artery (SCA) were spontaneously clipped via a right FL approach. Using MR imaging, the optic apparatus and tentorium were embodied along with other intracranial structures as 3D virtual and printed models (**Figure 2a-d**). According to the spatial relationship between the posterior clinoid process and SCA aneurysm, a good surgical approach could have been chosen.

Case 5: Three aneurysms at the right anterior choroidal artery (AChA) and ACA A1 and the left internal carotid artery (ICA0) were clipped simultaneously via a right LSO approach. The distal segment of the right ICA was formed from a rete mirabile, the proximal MCA was occluded with distal reconstitution with collaterals, and the right ACA A1 was tortuous. Using CTA and MR imaging, vascular structures with the rete mirabile and optic apparatus were realized as a 3D virtual model (**Figure 2e-g**). In fact, it was not clear preoperatively whether the contralateral ICA aneurysm could be clipped or not, a determination for which the 3D model would have been efficient.

IAs Requiring Intradural Bone Drilling

Case 6: Two aneurysms, at the right posterior communicating artery (PCoA) and MCA, respectively, were clipped via a right FL approach. Intradural drilling of the anterior clinoid process (ACP) was done for permanent clipping and probable proximal control. The 3D virtual and printed models were implemented with MR imaging for the optic apparatus and with CTA for the others (**Figure 3a-d**). A need for ACP drilling could be easily seen with the 3D model.

Case 7: A 12.1 mm right ICA aneurysm was clipped via a right LSO approach with intradural ACP drilling. These 3D virtual and printed models were made preoperatively with CTA and MR imaging (**Figure 3e-j**). With the aid of preoperative 3D models,

intradural ACP drilling and aneurysm clipping were determined. In addition, they were helpful preoperatively in choosing the proper clips and anticipating the direction of clip application. However, the orifices of the PCoA and AChA from the distal ICA visible on the 3DRA were too small to be expressed in the 3D model. If DSA had been used as raw data for segmentation instead of CTA or manual or semiautomated processing had been performed, fine orifices would have been shown on the 3D model.

Thrombosed Large IAs

Case 8: For a 24.5 mm ruptured and thrombosed ACoA aneurysm, aneurysmectomy, thrombus removal and aneurysmorrhaphy were performed via the subfrontal and interhemispheric approaches. It took a little time to identify the surrounding vessels and dissect both A2s from the sac based only on preoperative imaging. 3D virtual and printed models were made with CTA and MR imaging (**Figure 4a-d**). An intra-aneurysmal thrombus was also distinguished. Preoperative 3D models showing the whole aneurysm were helpful to understand the angioarchitecture and shorten the operation time.

Case 9: A left 19.3 mm thrombosed SCA aneurysm was treated with a left superficial temporal artery-SCA bypass and trapping of the left SCA just distal to the aneurysm via the subtemporal approach. The 3D models consisted of the skull base, aneurysm, intra-aneurysmal thrombus, tentorium and pons, excluding the cranial nerves, and were made with CTA, MR imaging and DSA (**Figure 4e-h**). The 3D models seemed useful to understand the spatial relationships of bone, pons, SCA and aneurysm. However, bridging veins and cranial nerves were not easy to realize because of the quality of the raw data.

Cavernous Malformations

Case 1: A 34.1 mm-sized CM located in the left thalamus was removed via the trans-insular approach. The 3D virtual and printed models were created with MR imaging alone (**Figure 5a-c**). Surface gyri and sulci were incorporated in the 3D virtual model but not in the 3D-printed model because diffuse reflection on the realistic-surface gyri and sulci can make it hard to look into the CM on the printed model. We expected both models to help intuitively determine an appropriate surgical approach and the patient's head position. However, they failed to realize the sylvian bridging veins and developmental venous anomaly located at the upper part of the CM.

Case 2: A 24.2 mm CM located in the pons was removed via the left retromastoid suboccipital approach. Only using MR imaging, the 5^{th}, 7^{th} and 8^{th} cranial nerves, brainstem, thalamus and tentorium, as well as the CM, were created as 3D virtual and printed models (**Figure 5d-f**). They seemed useful to understand the spatial relationship between the cranial nerves and CM on the surface of pons and to approach the CM via the left peritrigeminal safety zone on the pons. However, neural tracts and nuclei were still difficult to visualize in the models, except thick cranial nerves and major tracts such as the corticospinal tract, which can be represented with diffusion tensor MR tractography.

Arteriovenous Malformation

A ruptured AVM located in the right parietal lobe underwent preoperative embolization followed by surgical resection. The 3D models were created with CTA, MR imaging and DSA (**Figure 6**). Deep feeders from the AChA as well as superficial major feeders from the ACA, MCA and posterior cerebral artery were implemented. The 3D model would have been helpful in choosing the patient's position, choosing the size and location of the craniotomy, and disconnecting major feeders.

Discussion

With advancements in neurointervention and our knowledge of the natural history of cerebrovascular diseases, surgical cases are decreasing, and complex lesions are relatively more often referred to surgery. In addition, the best treatment outcomes with high-end surgical skills are demanding, as medicolegal problems frequently arise and incidental findings of risky lesions are increasing. Therefore, surgeons' proficiency as well as trainee education and explanations to the patients and their relatives have become more important than ever. For these purposes, 3D modeling is emerging as a good option. We made 3D virtual and printed models of surgical cerebrovascular diseases, including 9 IAs, 2 CMs and 1 AVM. The IA cases were selected because they simulated representative situations of clipping IAs. They consisted of 3 single lesions at common locations, 2 cases of multiple lesions necessitating a proper surgical approach, 2 IAs requiring intradural bone drilling, and 2 thrombosed cases calling for surgical plans other than clipping alone. Deeply seated CM cases were selected for the difficulty of approach and removal. One AVM case was chosen that required a 3-dimensional understanding of the relationship among feeders, nidus, draining veins and surrounding brain tissues. Through the 3D modeling of one prospective IA case, the surgical plan was changed. Although retrospectively implemented, it was not difficult to imagine how helpful 3D modeling would have been in intuitively understanding the surgical anatomy and making a plan if the other models have been made prospectively. It goes without saying that they would have been effective in educating the trainees and explaining the medical situations to the patients and their families. However, some limitations in 3D modeling have also been confirmed because of the limited quality of the raw imaging data and material properties.

Studies of 3D modeling for cerebrovascular diseases have been published since the late 1990s. IAs have been one of the representative targets.[4,7,8,10,12-15,17] The advantages of IA 3D modeling described in previous reports include trainee education in craniotomy; operative viewing and handling of the surgical devices; explanation to the patients and general public; and presurgical simulation, such as of craniotomy, intradural bone work

and selection of the clips. Some disadvantages are as follows: difficulty in visualizing atherosclerosis and calcification of the vessel walls; an unrealistic tactile sense of the tissues; and difficulty distinguishing small or thin tissues, such as vessels, cranial nerves and membranes. The most important procedure in aneurysm surgery is arachnoid dissection through the normal plane, which is still impossible. The smallest vessels implemented in the reports were 0.5 mm in diameter, and there was an attempt to clip the model aneurysm with a hollow structure.[10,12] Although hemodynamics cannot be simulated with the present techniques,[12] spontaneous rupture and bleeding from the model aneurysm have also been attempted.[13] In the beginning, long times to make models and high costs were pointed out;[4,8,14] however, manufacturing times and costs have recently been reduced.[5,6] A second common target disease is the AVM. The completeness of the AVM 3D models is less than that of the IA models.[4-6,11] They were implemented with only vascular structures and the skull. There was no attempt to make the brain parenchyma, vessels or bone. There has been no report of 3D modeling of cerebral CMs, although their modeling is considered similar to brain tumor modeling.

The results of this study are highly similar to those of previous reports, but this study has some points that stand out. First, it was clearly confirmed that our 3D modeling techniques are enough to simulate most of the situations encountered during aneurysm surgery except direct dissection and clipping. For example, they allow the selection of an appropriate approach and preoperative simulation, such as the contralateral approach for the aneurysm at the ACoA in Case 1, the proper kind of keyhole approach for the large MCA lesion in Case 2, the laterality and location of the MI approach for the lesion at the distal ACA in Case 3, the proper approach for the multiple IAs in Cases 4 and 5, and choosing intradural ACP drilling for the aneurysms at the PCoA and ICA in Cases 6 and 7, respectively. In particular, in prospective Case 7, the plan for ACP drilling changed from the extradural approach to the less invasive intradural approach, and the operation time was shortened based on the 3D virtual and printed models. If the aneurysm involved the cavernous segment of the ICA, alternative plans would have been made, such as wider exposure with extradural ACP drilling or bypass and endovascular trapping of the ICA harboring the aneurysm.[17] Second, we have the technical know-how

to make a transparent brain tissue. Using a transparent brain model can be helpful in identifying the angioarchitecture of the lesions inside the brain, making a proper craniotomy toward the target lesions and localizing the right dissection plane to preserve the adjacent eloquent brain like using a navigation system. Diffuse reflection by the convoluted surface can interfere with seeing the structures within the brain, so how much of the sulcus and gyrus to include should be determined according to the purpose of the 3D modeling. Third, using merging techniques of different raw imaging data, some specific structures not shown in previous reports, such as thrombi, major cranial nerves and the dural layer of the falx and tentorium, could be made, although the merging process has not yet been fully automated. Most of the previous studies used only one imaging dataset among MR, CT and DSA.[5,6,8,10] CTA and DSA are advantageous in segmenting bone, calcifications and vessels, and MR imaging is better for soft tissue segmentation, such as scalp, muscle, brain tissue, cranial nerves, dural membrane, thrombus and major arterial and venous sinuses. Intra-aneurysmal thrombi could be made in Cases 8 and 9 with CTA, DSA and MR imaging. Major cranial nerves could be made based on MR imaging, for example, optic nerves in IA Cases 4-7 and trigeminal and facial/vestibulocochlear nerves in CM Case 2. Tentorium was also manually implemented in Cases 4 and 9. Fully automated processing of the merging of different imaging data is expected to reduce the manufacturing time and facilitate the prospective application of 3D modeling.

The limitations mentioned above should be overcome in the near future as imaging tools, materials and modeling techniques progress. Completely realistic 3D modeling techniques would help to discriminate fine structures such as small vessels and cranial nerves, thin arachnoid membranes, en passage vessels from real feeders in AVMs, and CM from developmental venous anomalies, as well as to simulate the main procedures directly. In addition, 3D virtual modeling is expected to be applied to intraoperative virtual and augmented reality techniques and robotic neurosurgery. Although not applied in this study, functional neuroanatomy could be realized in the 3D virtual and printed models using functional MR and MR tractography.

There were some limitations in this study. Only 12 cases were made as 3D virtual and printed models. Except for 1 case, they all were retrospectively made, based on which their usefulness was speculated. Most of the vessels up to 1 mm in diameter were implemented. Approximately 0.2 mm vessels could be made; however, these were thought to be useless if the other small or thin tissues were not made together. The time to make each 3D-printed model was not measured. Approximately 3 or 4 days per printed model was necessary in this study. Some reports say that 8 to 18 hours was spent,[5,6] but that was for the vasculature alone. Therefore, a few days still seems to be needed for one model.

Conclusions

The virtual and printed models of IAs, CMs and AVMs, as representative cerebrovascular diseases, were satisfactorily implemented in this study. The physicians easily saw how helpful the human skull model was for the craniotomy and surgical approach. 3D modeling goes beyond a simple skull model and helps to intuitively observe various intracranial structures, such as the brain, vessels and pathologic lesions. In the near future, substantial progress is expected to be made in the neurosurgical field in terms of education, training, explanation and treatment, although there are still some limitations in the imaging data, materials and 3D modeling techniques.

References

1. Hull, C. W. inventor; Uvp, Inc. San Gabriel, Calif., assignee. Apparatus for production of three-dimensional objects by stereolithography. United States Patent US Patent 4,575,330. 1986 Mar 11.

2. Ventola, C. L. Medical applications for 3D printing: current and projected uses. *Pharmacy and Therapeutics* **39**, 704 (2014).

3. Randazzo, M., Pisapia, J. M., Singh, N. & Thawani, J. P. 3D printing in neurosurgery: a systematic review. *Surgical Neurology International* **7**, S801 (2016).

4. D'Urso, P. S. *et al.* Cerebrovascular biomodelling: a technical note. *Surgical neurology* **52**, 490-500 (1999).

5. Weinstock, P., Prabhu, S. P., Flynn, K., Orbach, D. B. & Smith, E. Optimizing cerebrovascular surgical and endovascular procedures in children via personalized 3D printing. *Journal of Neurosurgery: Pediatrics* **16**, 584-589 (2015).

6. Conti, A. *et al.* 3D-printing of arteriovenous malformations for radiosurgical treatment: pushing anatomy understanding to real boundaries. *Cureus* **8** (2016).

7. Andereggen, L. *et al.* Stereolithographic models in the interdisciplinary planning of treatment for complex intracranial aneurysms. *Acta neurochirurgica* **158**, 1711-1720 (2016).

8. Kimura, T. *et al.* Simulation of and training for cerebral aneurysm clipping with 3-dimensional models. *Neurosurgery* **65**, 719-726 (2009).

9. Panesar, S. S. *et al.* Patient-specific 3-dimensionally printed models for neurosurgical planning and education. *Neurosurgical focus* **47**, E12 (2019).

10. Ryan, J. R., Almefty, K. K., Nakaji, P. & Frakes, D. H. Cerebral aneurysm clipping surgery simulation using patient-specific 3D printing and silicone casting. *World neurosurgery* **88**, 175-181 (2016).

11. Ye, X. *et al.* A three-dimensional color-printed system allowing complete modeling of arteriovenous malformations for surgical simulations. *Journal of Clinical Neuroscience* (2020).

12. Lan, Q., Zhu, Q., Xu, L. & Xu, T. Application of 3D-Printed Craniocerebral Model in Simulated Surgery for Complex Intracranial Lesions. *World Neurosurgery* **134**, e761-e770 (2020).

13. Kumagai, K., Mori, K., Takeuchi, S. & Wada, K. Surgical training for the management of intraoperative aneurysm rupture using a three-dimensional artificial model. *Asian journal of neurosurgery* **14**, 172 (2019).

14. Wurm, G., Tomancok, B., Pogady, P., Holl, K. & Trenkler, J. Cerebrovascular stereolithographic biomodeling for aneurysm surgery. *Journal of neurosurgery* **100**, 139-145 (2004).

15. Kim, P. S. *et al.* Obtaining informed consent using patient specific 3D printing cerebral aneurysm model. *Journal of Korean Neurosurgical Society* **62**, 398 (2019).

16. Cho, W.-S. *et al.* Keyhole approach and neuroendoscopy for cerebral aneurysms. *Journal of Korean Neurosurgical Society* **60**, 275 (2017).

17. Okonogi, S. *et al.* Operative simulation of anterior clinoidectomy using a rapid prototyping model molded by a three-dimensional printer. *Acta Neurochirurgica* **159**, 1619-1626 (2017).

Acknowledgements

This research was supported by a grant of the Korea Health Technology R&D Project through the Korea Health Industry Development Institute (KHIDI), funded by the Ministry of Health & Welfare, Republic of Korea (grant number: HI20C2092).

Author Contributions

- Concept and design: Sang Joon Park, Won-Sang Cho, Chul-Kee Park
- Data acquisition: Da Yeong Lee, Chang Hwan Pang, Doohee Lee
- Data analysis and interpretation: Jin Woo Bae, Won-Sang Cho
- Drafting the article: Jin Woo Bae, Won-Sang Cho
- Article revision for important intellectual content: Jeong Eun Kim. Won-Sang Cho
- Review and final approval of manuscript revisions: Sang Joon Park, Won-Sang Cho

Additional Information

Competing interests:

Sang Joon Park is founder and CEO of MEDICALIP.

Chul-Kee Park owns stock options in MEDICALIP.

The other authors have no conflict of interest to declare.

Figure Legends

Figure 1. Single IAs. Case 1 (**a** and **b**): An aneurysm (*single arrow*) arising at the ACoA was identified on the 3DRA (**a**) and on the 3D virtual model (**b**). Case 2 (**c-f**): a large aneurysm at the right MCA bifurcation was identified on the anterior and posterior aspects of the 3DRA (**c and d**, respectively). The 3D virtual model showed an anterior aspect of the whole cerebrovasculature (**e**) and magnified posterior aspect of the aneurysm (**f**), in which each component, such as the artery, vein, brain and skull, could be set to various opacities with the right-hand buttons of the MODIP®. Case 3 (**g-i**): An aneurysm (*double arrows*) at the right distal ACA was demonstrated on the 3DRA (**g**), 3D virtual (**h**) and printed models (**i**).

Figure 2. Multiple IAs. Case 4 (**a-d**): Two aneurysms, at the right MCA (*single arrow*) and SCA (double arrows), are shown on the 3DRA (**a and b**, respectively), 3D virtual model (**c**), and 3D-printed model (**d**). On the 3D virtual and printed models, tentorium (*sky blue*) and optic nerves (*yellow*) could also be implemented. Case 5 (**e-g**): Three aneurysms, at the left ICA (*single arrow*), right ACA (*double arrows*) and AChA (*triple arrows*), were demonstrated on the 3DRA (**e and f**) and 3D virtual model (**g**). The terminus of the right ICA was formed from the rete mirabile (**f and g**).

Figure 3. IAs requiring intradural bone drilling. Case 6 (**a-d**): Two aneurysms were shown, at the right MCA (*single arrow*) and PCoA (*double arrows*), on the 3DRA (**a**), one 3D virtual model (**b**), the other virtual model with partial opacification to the skull (**c**) and the printed model (**d**). The right ACP (*arrowheads*) covering the PCoA and aneurysm was identified (**c and d**). Case 7 (**e-j**): a large aneurysm (*single arrows*) at the right ICA was identified on 3DRA (**e**) and the 3D virtual (**f**) and printed models (**g**). Right ACP (*arrowheads*) covered the aneurysm (**f and h**). Intradural drilling of the ACP and cutting of the distal dural ring exposed the anterior margin of the aneurysm neck

(*dotted arrow*; **i**), and the aneurysm was completely clipped with a tandem clipping technique (**j**).

Figure 4. Thrombosed large IAs. Case 8 (**a-d**): A large thrombosed aneurysm at the ACoA was identified on the 3DRA (**a**), T1-enhanced axial MR images (**b**), and the 3D virtual (**c**) and printed models (**d**). The intraluminal part of the aneurysm (*single arrows*) and intrasaccular thrombus (*dotted single arrows*) were distinguished. Case 9 (**e-h**): a large thrombosed aneurysm at the left SCA compressing the left pons was identified on the 3DRA (**e**), T1-enhanced sagittal MR images (**f**), 3D virtual model (**g**), and 3D-printed model (**h**). The intraluminal part (*single arrows*) and intrasaccular thrombus (*dotted single arrows*) are shown.

Figure 5. Deep-seated CMs. Case 1 (**a-c**): A CM at the left thalamus was identified on the T2-weighted axial MR image (**a**), 3D virtual model (**b**), and 3D-printed model (**c**). The left MCA and superficial sylvian veins were demonstrated together, and the brain parenchyma was made transparently without a sulcus or gyrus except the sylvan fissure to prevent diffuse reflection. Case 2 (**d-f**): a CM (*single arrow*) at the left pons was presented on the T2-weighted axial MR image (**d**), 3D virtual model (**e**), and 3D-printed model (**f**), for which the intracranial structure model was extracted from the skull model for the presentation. The thalamus, brainstem, 5^{th}, 7^{th} and 8^{th} cranial nerves and tentorium were well visualized.

Figure 6. An AVM located at the right parietal lobe was identified on the DSA (**a-c**), T1-enhanced sagittal MR image (**d**), 3D virtual model (**e**), and 3D-printed model (**f**). It was fed from the ACA (*single arrow*), MCA (*double arrows*), PCA (*triple arrows*), AChA (*dotted single arrow*), medial posterior choroidal artery (*dotted double arrows*) and posterior splenial artery (*dotted triple arrows*). All the major feeders from the ACA, MCA, PCA and ICA were made on the 3D virtual and printed models.

Figure 1.

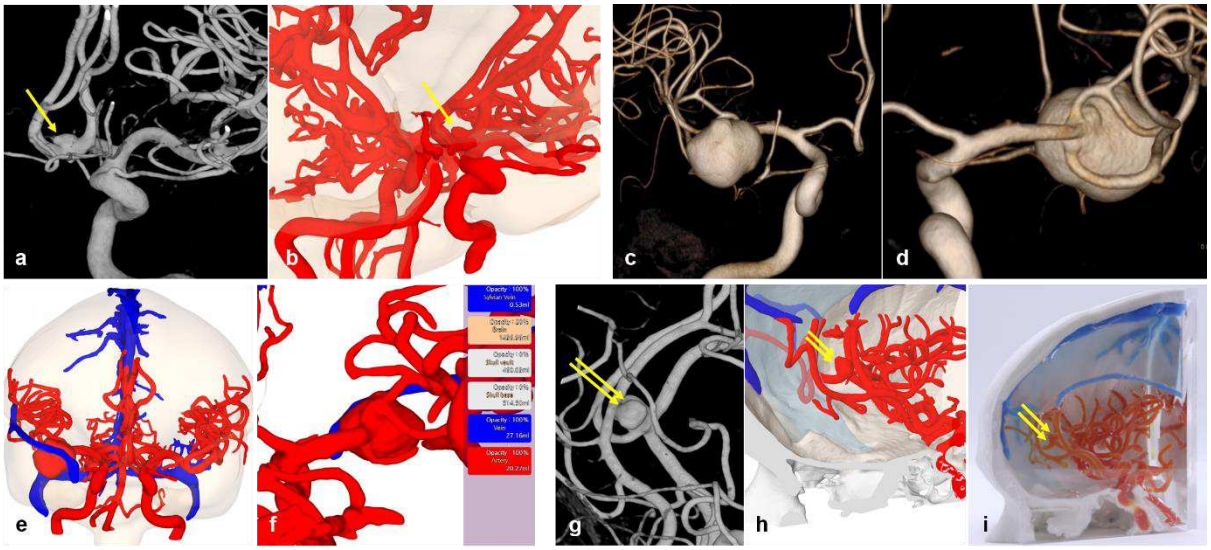

Figure 2.

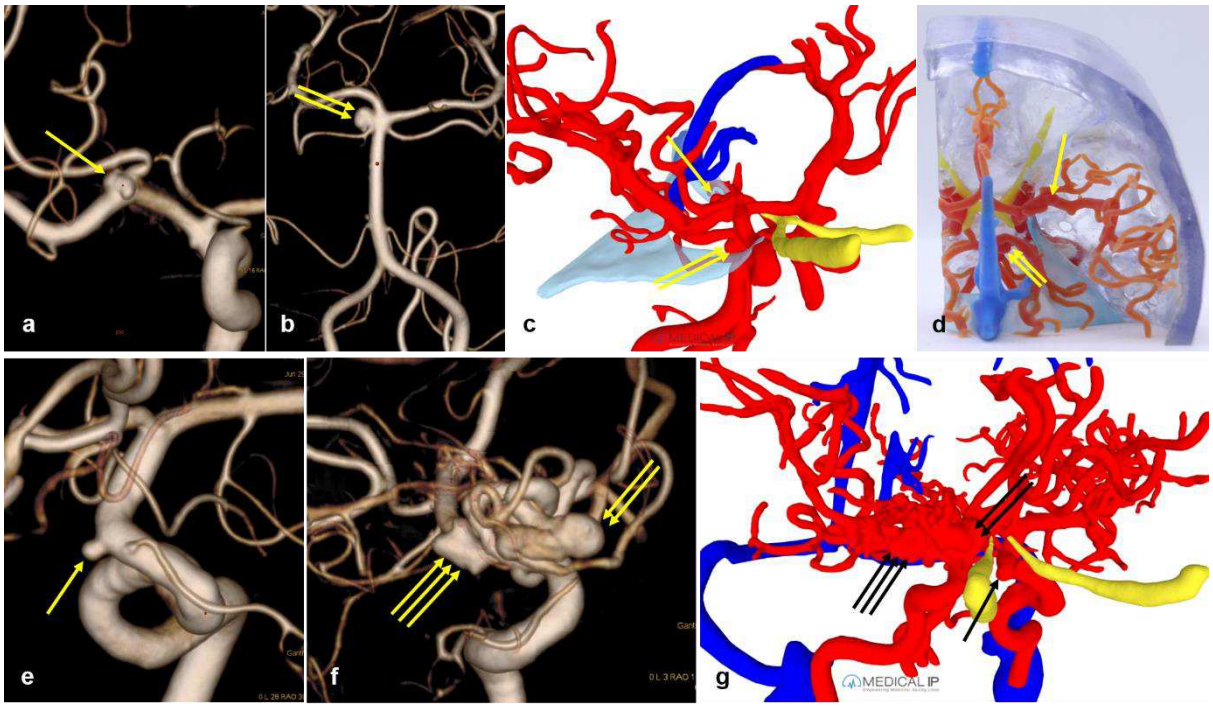

Figure 3.

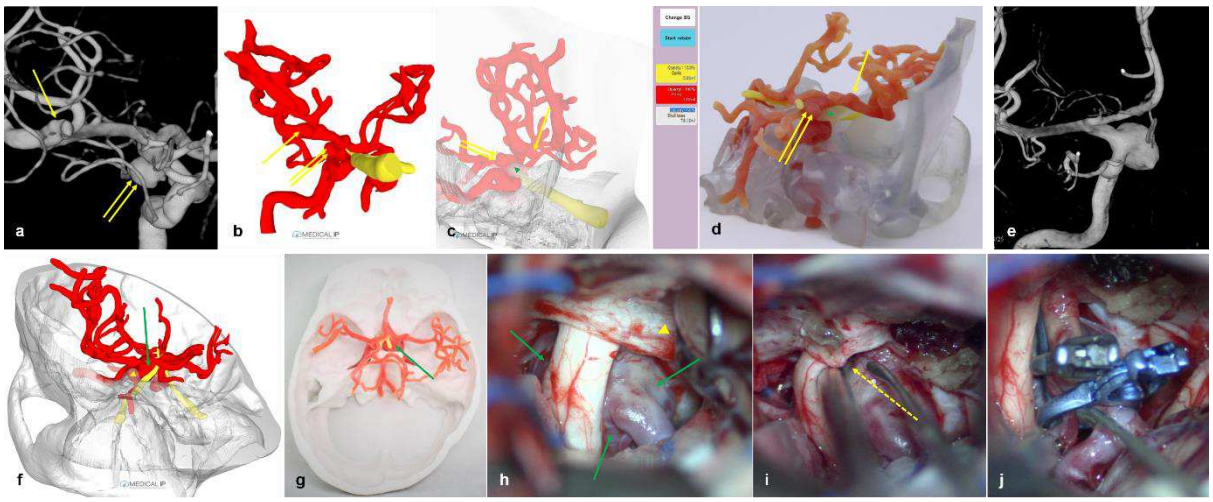

Figure 4.

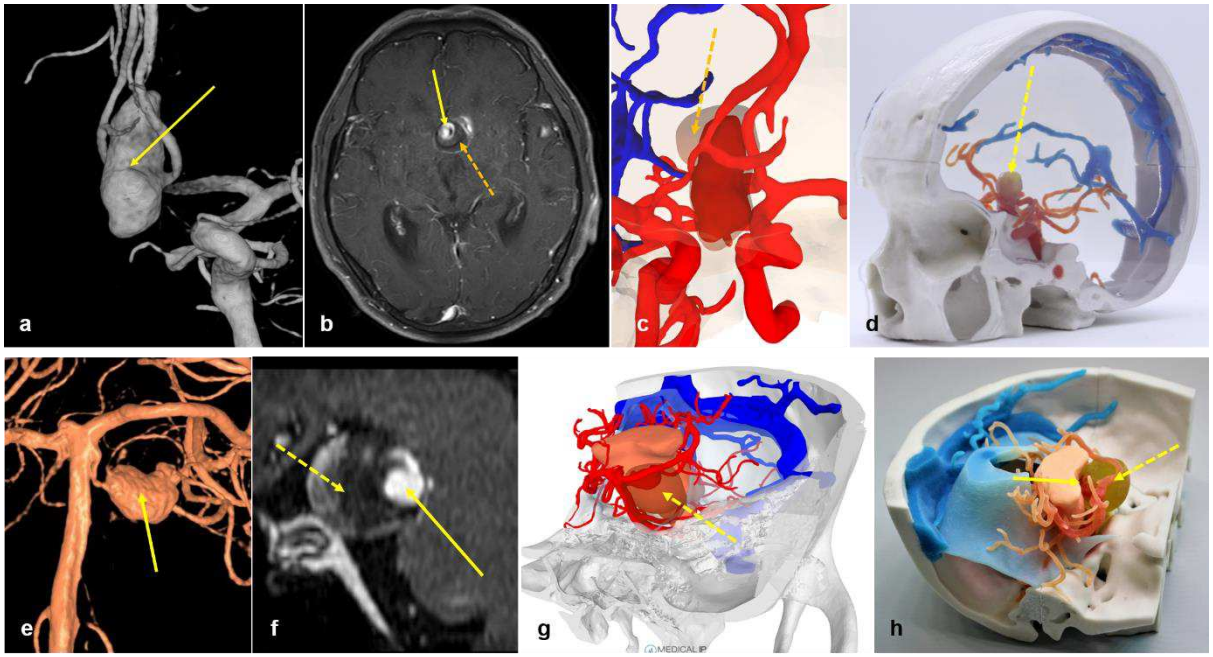

Figure 5.

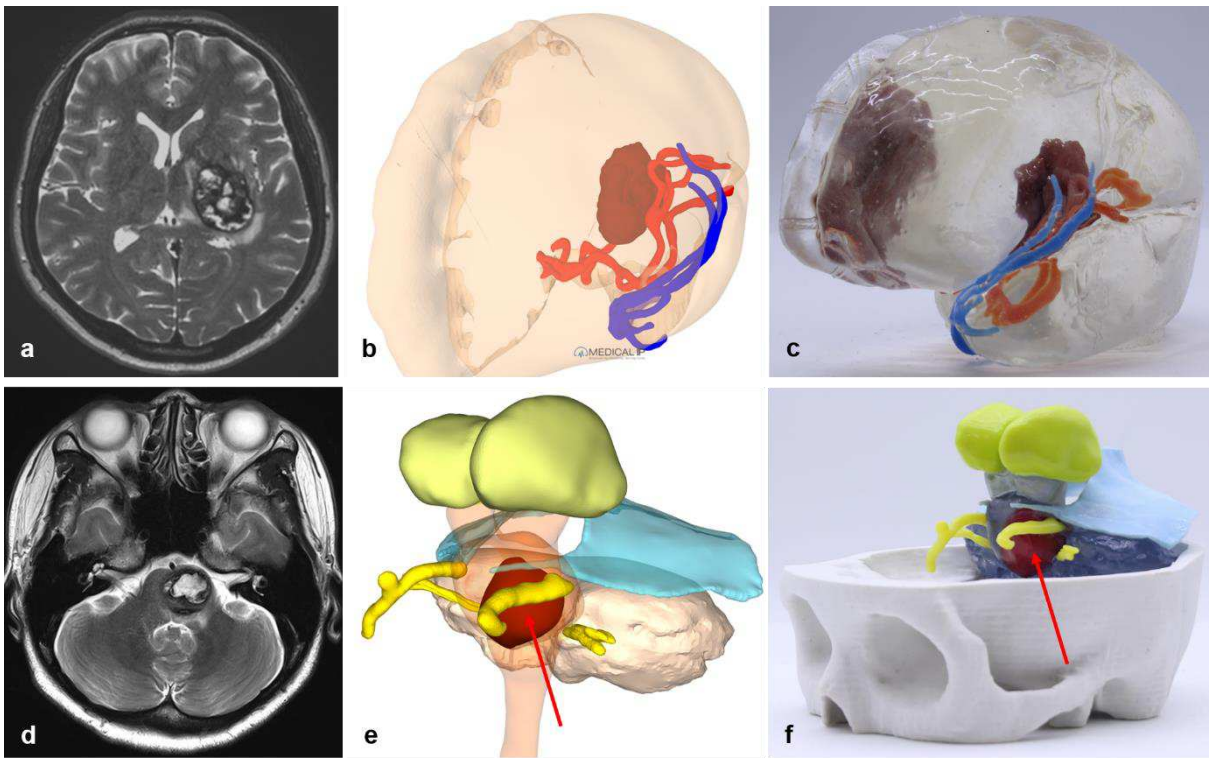

Figure 6.

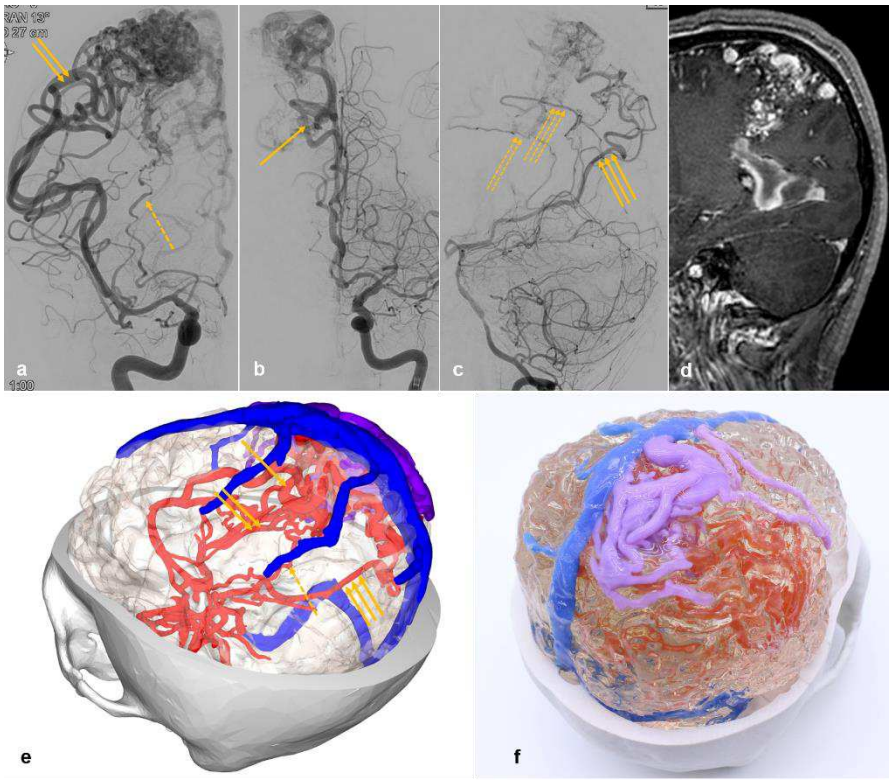

Table. Baseline characteristics of the representative cerebrovascular cases with hyperlinks of their 3D virtual and printed models.

Case no.	Age /Sex	Locations (maximal diameter, mm)	Preoperative status	Operations	Modelling period	3D virtual models for simulation	3D virtual models for printing
Aneurysms							
1	49/F	ACoA (4.3)	Unruptured	Clipping via one keyhole	Retrospective	http://147.47.229.147:8080/STLRendering/191219_acoa_model.html	None
2	60/M	R MCA (17.2)	Unruptured	Clipping via one keyhole	Retrospective	http://147.47.229.147:8080/STLRendering/200108_PHG.html	None
3	70/F	R ACA (9.1)	Unruptured	Clipping via one keyhole	Retrospective	http://147.47.229.147:8080/STLRendering/200123_YDI_OPEN.html	http://147.47.229.147:8080/STLRendering/200206_YDI_PRINT.html
4	51/F	R MCA (4.4), R SCA (5.1)	Unruptured	Clipping via one keyhole	Retrospective	http://147.47.229.147:8080/STLRendering/200219_SHJ.html	http://147.47.229.147:8080/STLRendering/200312_SHJ_PRINT.html
5	47/F	R AChA (6.5), R ACA (4.0), L ICA (2.5)	Unruptured	Clipping via one keyhole	Retrospective	http://147.47.229.147:8080/STLRendering/200305_KHG.html	None
6	67/F	R PCoA (5.1), R MCA (3.9)	Unruptured	Clipping via one keyhole, intradural ACP drilling	Retrospective	http://147.47.229.147:8080/STLRendering/200211_CDS.html	http://147.47.229.147:8080/STLRendering/200302_CDS_PRINT.html
7	51/F	R ICA (12.1)	Unruptured	Clipping via one keyhole, intradural ACP drilling	Prospective	http://147.47.229.147:8080/STLRendering/200515_KSO.html	http://medicalip.synology.me:8080//STLRendering/200609_KSO_print.html
8	65/M	ACoA (24.5)	Ruptured, partially thrombosed	Aneurysmorrhaphy via subfrontal and interhemispheric approach	Retrospective	http://147.47.229.147:8080/STLRendering/200317_CJY.html	

							http://147.47.229.147:8080/STLRendering/200407_CJY_print-2.html
9	59/F	L SCA (19.3)	Mass effect, partially thrombosed	STA-SCA bypass and distal SCA trapping via subtemporal approach	Retrospective	http://147.47.229.147:8080/STLRendering/200316_KMH.html http://147.47.229.147:8080/STLRendering/200428_KMH_TFCA.html	http://147.47.229.147:8080/STLRendering/200428_KMH.html http://medicalip.synology.me:8080//STLRendering/200507_KMH_print.html
Cavernous malformations							
1	43/F	L thalamus (34.1)	Repeat bleeding	Removal via trans-insular approach	Retrospective	http://147.47.229.147:8080/STLRendering/200420_SHJ.html	http://147.47.229.147:8080/STLRendering/200507_SHJ_print.html
2	32/F	L pons (24.2)	Repeat bleeding	Removal via retromastoid suboccipital craniotomy	Retrospective	http://medicalip.synology.me:8080//STLRendering/200519_JHW.html	http://medicalip.synology.me:8080//STLRendering/200610_JHW_print.html
Arteriovenous malformation							
1	34/F	R parietal lobe (50.1)	Bleeding	Removal via parietal craniotomy	Retrospective	http://medicalip.synology.me:8080/STLRendering/200526_OYM.html	http://medicalip.synology.me:8080//STLRendering/200609_OYM_print.html

ACoA, anterior communicating artery; R, right; MCA, middle cerebral artery; ACA, anterior cerebral artery; PCoA, posterior communicating artery; AChA, anterior choroidal artery; L, left; ICA, internal carotid artery; SCA, superior cerebellar artery; ACP, anterior clinoid process; STA, superficial temporal artery

Figures

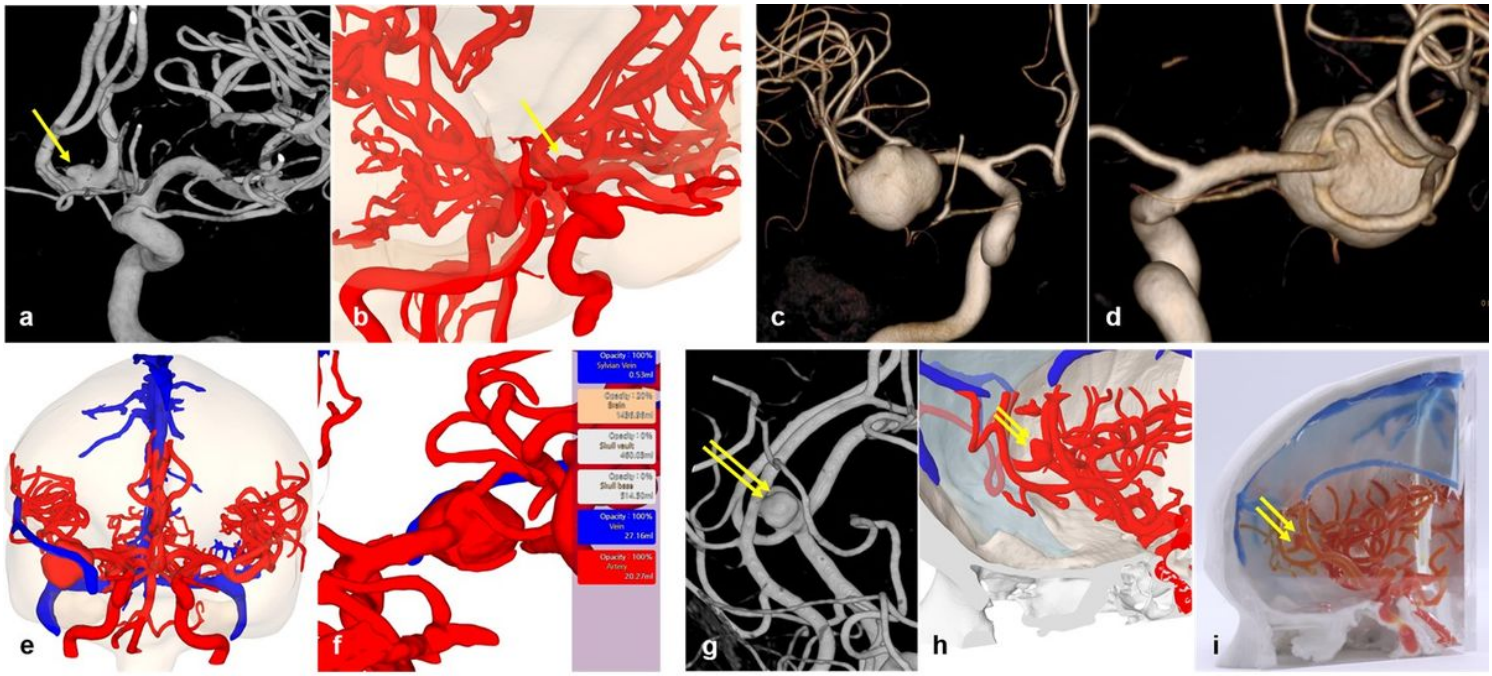

Figure 1

Single IAs. Case 1 (a and b): An aneurysm (single arrow) arising at the ACoA was identified on the 3DRA (a) and on the 3D virtual model (b). Case 2 (c-f): a large aneurysm at the right MCA bifurcation was identified on the anterior and posterior aspects of the 3DRA (c and d, respectively). The 3D virtual model showed an anterior aspect of the whole cerebrovasculature (e) and magnified posterior aspect of the aneurysm (f), in which each component, such as the artery, vein, brain and skull, could be set to various opacities with the right-hand buttons of the MODIP®. Case 3 (g-i): An aneurysm (double arrows) at the right distal ACA was demonstrated on the 3DRA (g), 3D virtual (h) and printed models (i).

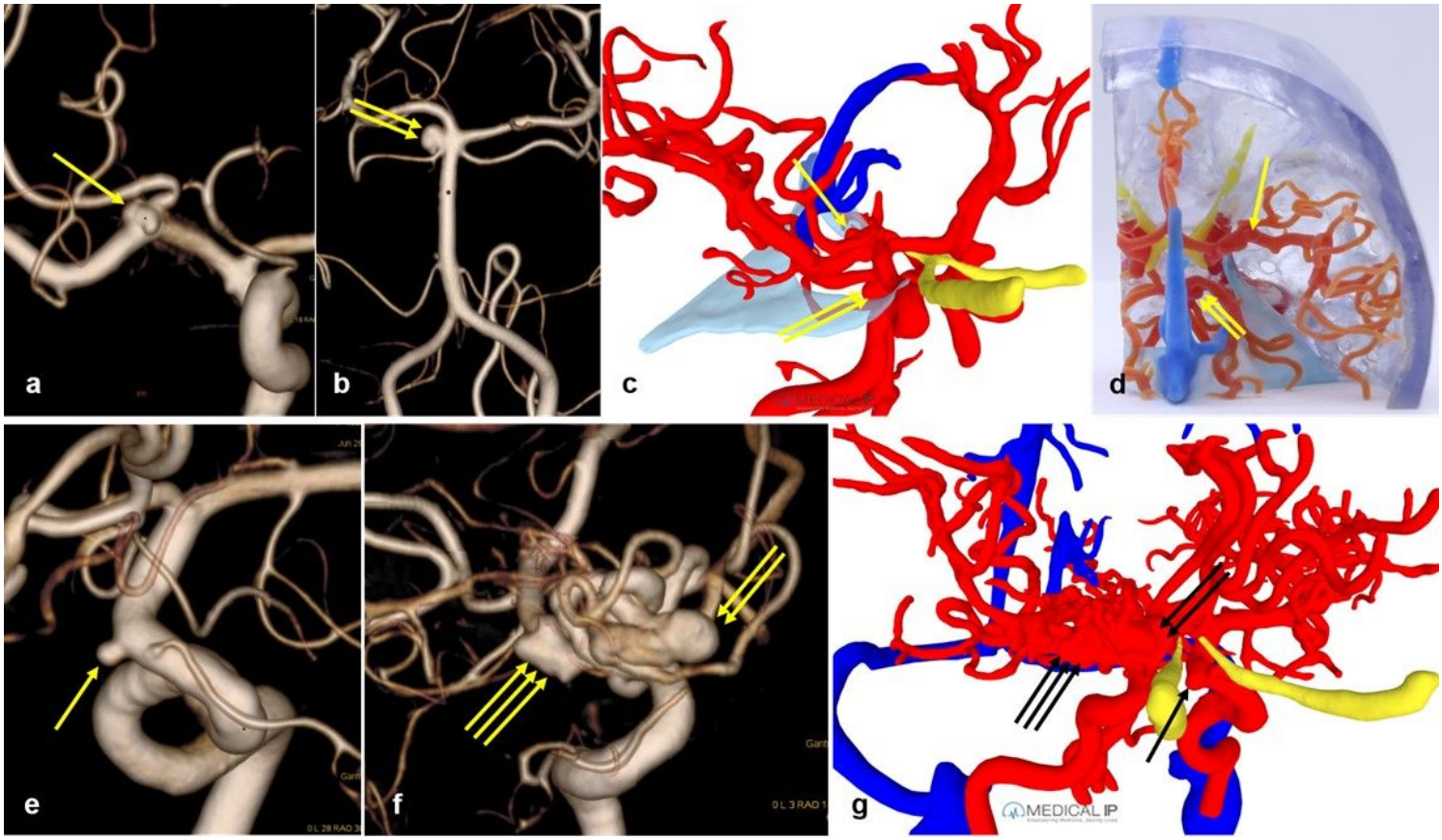

Figure 2

Multiple IAs. Case 4 (a-d): Two aneurysms, at the right MCA (single arrow) and SCA (double arrows), are shown on the 3DRA (a and b, respectively), 3D virtual model (c), and 3D-printed model (d). On the 3D virtual and printed models, tentorium (sky blue) and optic nerves (yellow) could also be implemented. Case 5 (e-g): Three aneurysms, at the left ICA (single arrow), right ACA (double arrows) and AChA (triple arrows), were demonstrated on the 3DRA (e and f) and 3D virtual model (g). The terminus of the right ICA was formed from the rete mirabile (f and g).

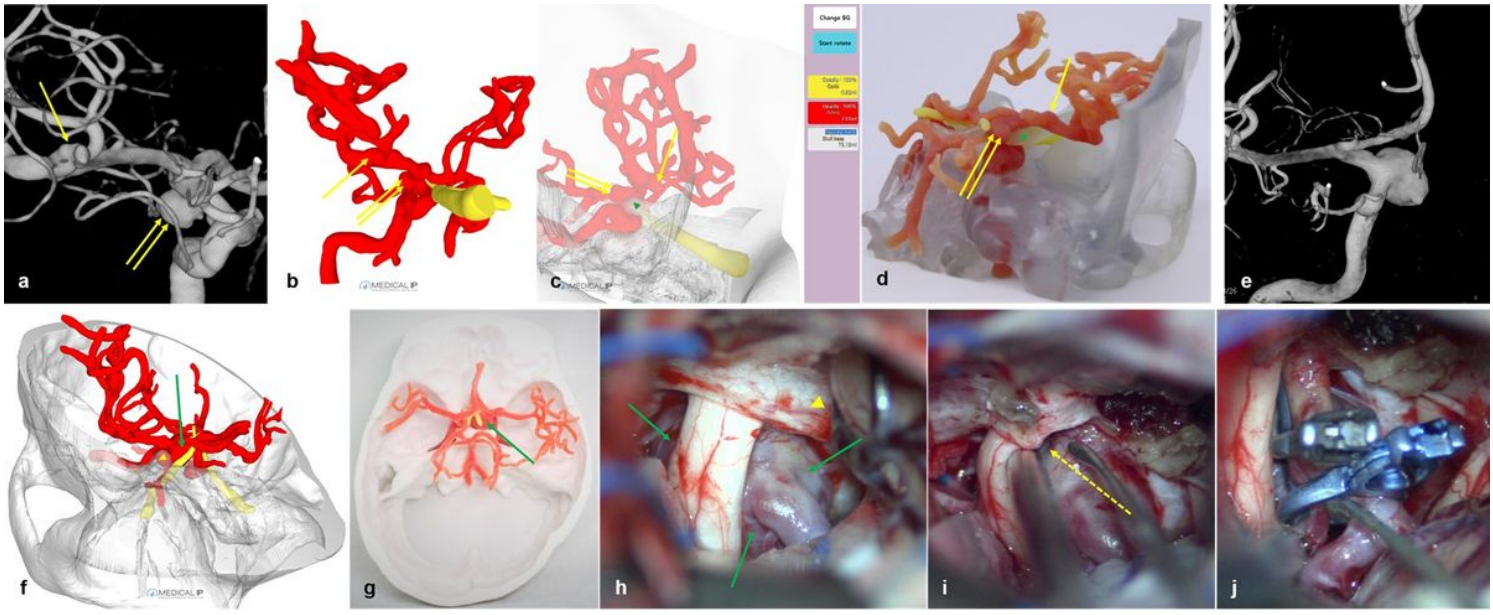

Figure 3

IAs requiring intradural bone drilling. Case 6 (a-d): Two aneurysms were shown, at the right MCA (single arrow) and PCoA (double arrows), on the 3DRA (a), one 3D virtual model (b), the other virtual model with partial opacification to the skull (c) and the printed model (d). The right ACP (arrowheads) covering the PCoA and aneurysm was identified (c and d). Case 7 (e-j): a large aneurysm (single arrows) at the right ICA was identified on 3DRA (e) and the 3D virtual (f) and printed models (g). Right ACP (arrowheads) covered the aneurysm (f and h). Intradural drilling of the ACP and cutting of the distal dural ring exposed the anterior margin of the aneurysm neck (dotted arrow; i), and the aneurysm was completely clipped with a tandem clipping technique (j).

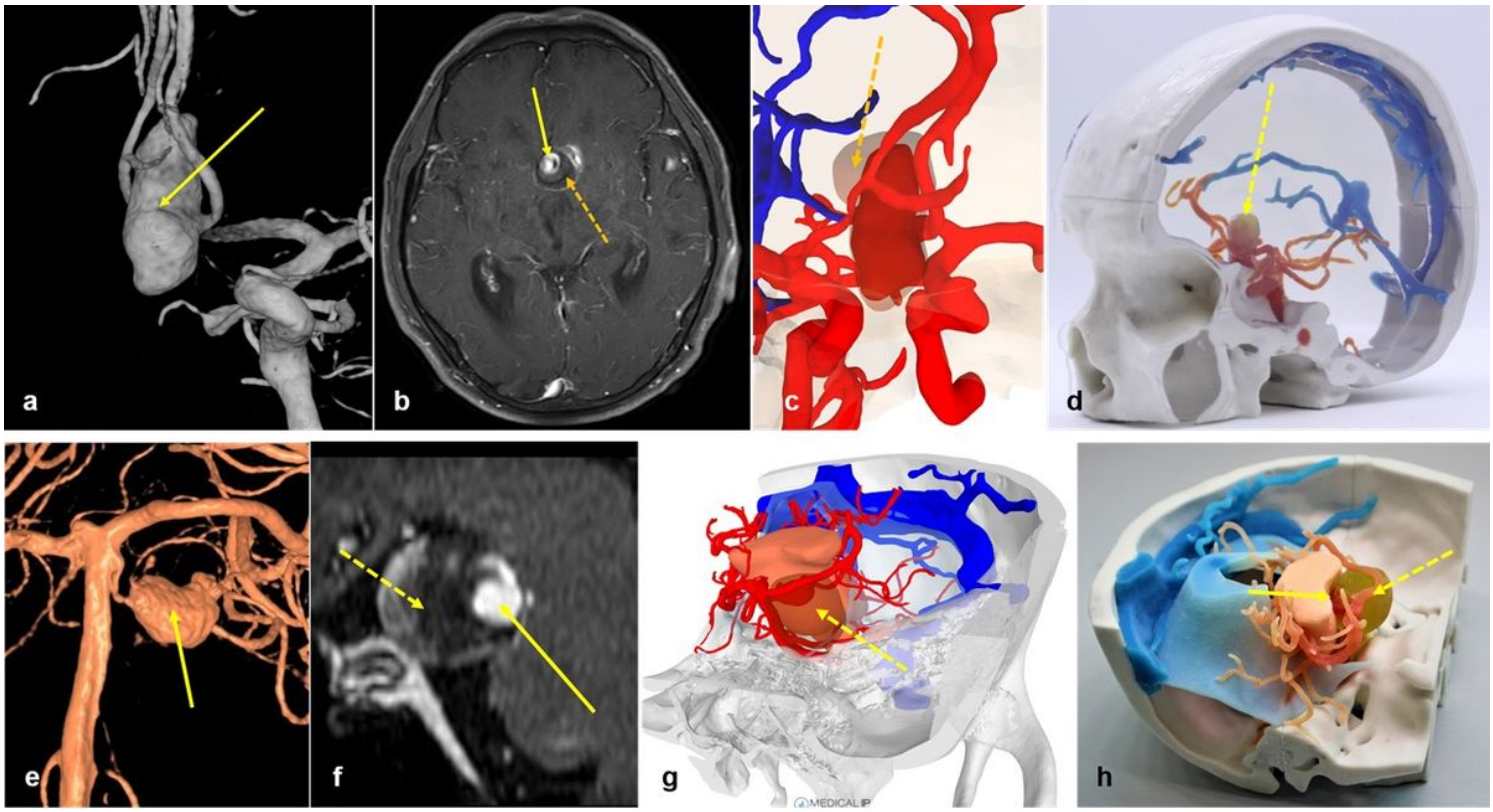

Figure 4

Thrombosed large IAs. Case 8 (a-d): A large thrombosed aneurysm at the ACoA was identified on the 3DRA (a), T1-enhanced axial MR images (b), and the 3D virtual (c) and printed models (d). The intraluminal part of the aneurysm (single arrows) and intrasaccular thrombus (dotted single arrows) were distinguished. Case 9 (e-h): a large thrombosed aneurysm at the left SCA compressing the left pons was identified on the 3DRA (e), T1-enhanced sagittal MR images (f), 3D virtual model (g), and 3D-printed model (h). The intraluminal part (single arrows) and intrasaccular thrombus (dotted single arrows) are shown.

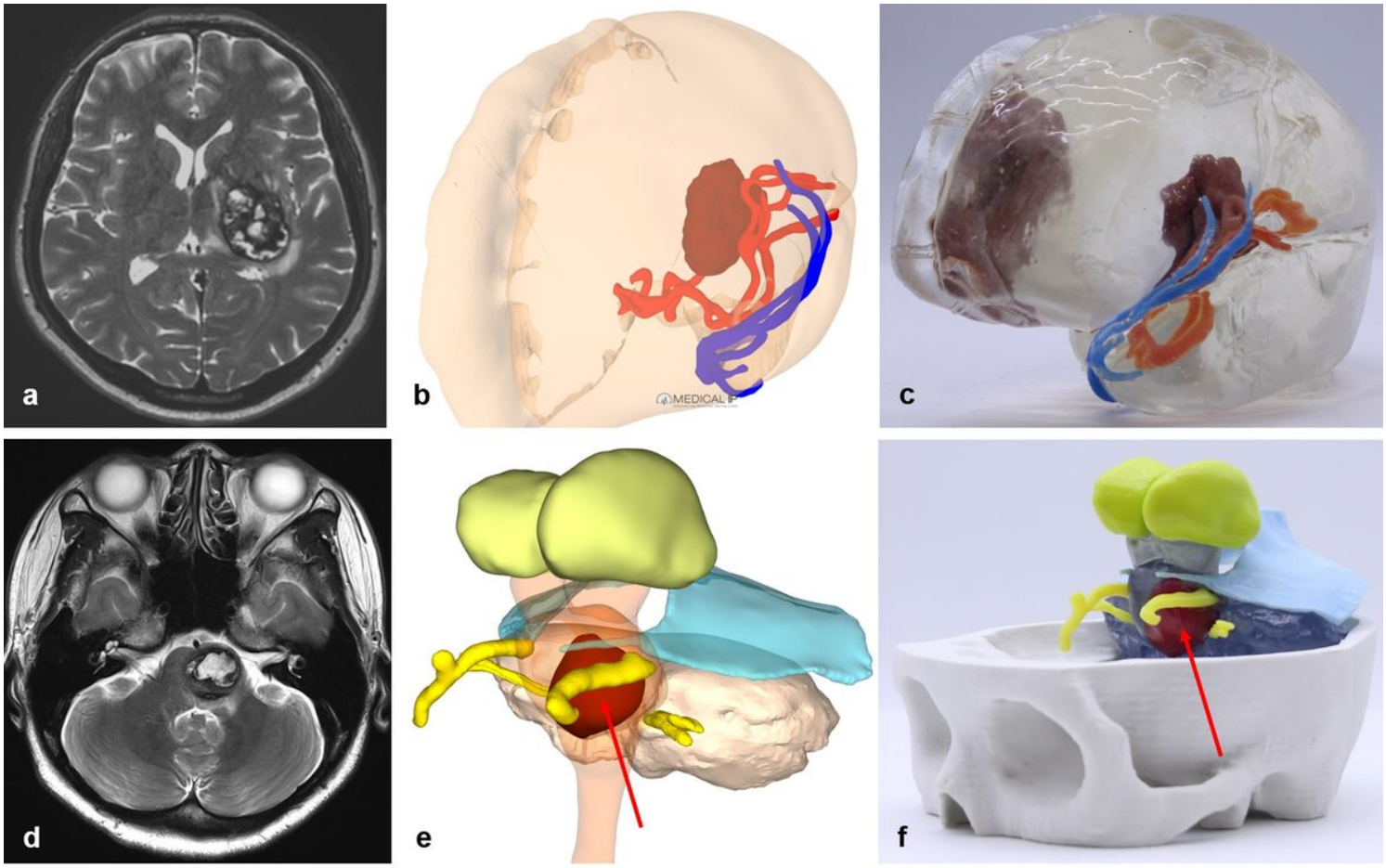

Figure 5

Deep-seated CMs. Case 1 (a-c): A CM at the left thalamus was identified on the T2-weighted axial MR image (a), 3D virtual model (b), and 3D-printed model (c). The left MCA and superficial sylvian veins were demonstrated together, and the brain parenchyma was made transparently without a sulcus or gyrus except the sylvan fissure to prevent diffuse reflection. Case 2 (d-f): a CM (single arrow) at the left pons was presented on the T2-weighted axial MR image (d), 3D virtual model (e), and 3D-printed model (f), for which the intracranial structure model was extracted from the skull model for the presentation. The thalamus, brainstem, 5th, 7th and 8th cranial nerves and tentorium were well visualized.

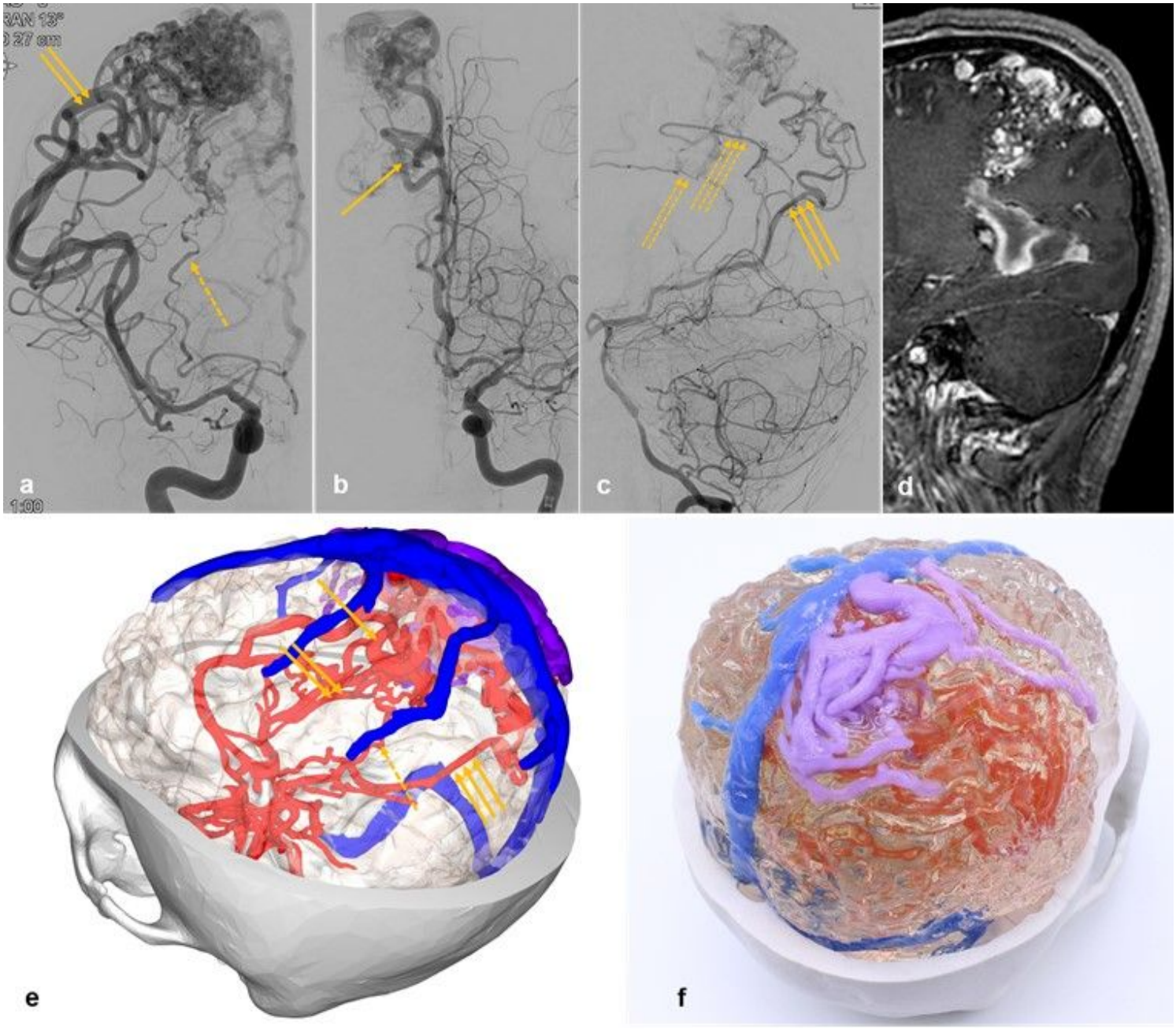

Figure 6

An AVM located at the right parietal lobe was identified on the DSA (a-c), T1-enhanced sagittal MR image (d), 3D virtual model (e), and 3D-printed model (f). It was fed from the ACA (single arrow), MCA (double arrows), PCA (triple arrows), AChA (dotted single arrow), medial posterior choroidal artery (dotted double arrows) and posterior splenial artery (dotted triple arrows). All the major feeders from the ACA, MCA, PCA and ICA were made on the 3D virtual and printed models.